Title
Possible electric field induced indirect to direct band gap transition in MoSe2

Permalink
https://escholarship.org/uc/item/4pb7z68n

Authors
Kim, BS
Kyung, WS
Seo, JJ
et al.

SCIENTIFIC REPORTS

Possible electric field induced indirect to direct band gap transition in MoSe$_2$

B. S. Kim[1,2,3], W. S. Kyung[2,4], J. J. Seo[2,5], J. Y. Kwon[1,2], J. D. Denlinger[4], C. Kim[1,2] & S. R. Park[3]

Direct band-gap semiconductors play the central role in optoelectronics. In this regard, monolayer (ML) MX$_2$ (M = Mo, W; X = S, Se) has drawn increasing attention due to its novel optoelectronic properties stemming from the direct band-gap and valley degeneracy. Unfortunately, the more practically usable bulk and multilayer MX$_2$ have indirect-gaps. It is thus highly desired to turn bulk and multilayer MX$_2$ into direct band-gap semiconductors by controlling external parameters. Here, we report angle-resolved photoemission spectroscopy (ARPES) results from Rb dosed MoSe$_2$ that suggest possibility for electric field induced indirect to direct band-gap transition in bulk MoSe$_2$. The Rb concentration dependent data show detailed evolution of the band-gap, approaching a direct band-gap state. As ionized Rb layer on the surface provides a strong electric field perpendicular to the surface within a few surface layers of MoSe$_2$, our data suggest that direct band-gap in MoSe$_2$ can be achieved if a strong electric field is applied, which is a step towards optoelectronic application of bulk materials.

Whether a semiconductor has a direct or indirect band-gap greatly affects its optical properties; excitons in direct band-gap semiconductors, for example, strongly couple to photons. For such reason, direct band-gap semiconductors can be used for optoelectronic applications such as light emitting and laser diodes[1, 2]. Monolayer 2H-MX$_2$ (M = Mo, W; X = S, Se) also have a direct band-gap and have drawn considerable attention due to their novel electronic properties as described by the Massive Dirac-Fermion model[3, 4]. The coupling between the valley degree of freedom and circularly polarized light opened the field of valley Hall effect[5, 6]. Such intriguing physics can be realized only in 1 ML 2H-MX$_2$ because multi-layer 2H-MX$_2$ has an indirect band gap and thus does not strongly couple to light. Photoluminescence and photo absorption spectroscopy experiments indeed show that photon-exciton coupling is strong only in 1 ML 2H-MX$_2$[7–10].

Making bulk MX$_2$ a direct gap material would be highly desirable because the necessity for high quality ML MX$_2$ puts severe limitation on the actual application. There were many computational or experimental studies in search of a way to control the band structure and gap size in bulk 2H-MX$_2$. It was found that the band gap size of TMDs can be modified by using various methods such as strain[11–17], chemical doping[18–22], electric field[12, 23–26], making heterostructures[12, 27–31] and using different substrates for thin films[32–35]. However, there has not been any proposal to induce direct band gap in bulk MX$_2$.

Alkali metal atoms evaporated on the surface of a sample not only dope electrons to the sample but also generate a strong electric field near surface[36]. Our strategy to the issue of inducing a direct gap is to apply a strong electric field perpendicular to the MoSe$_2$ layers by using such alkali metal dosing. Valence band dispersions and conduction band minimum (CBM) were measured by angle-resolved photoemission spectroscopy (ARPES). The indirect gap which is about 0.2 eV smaller than the direct gap in bulk MoSe$_2$ is greatly reduced after alkali metal dosing, almost to the point of indirect to direct gap transition. Our observation casts a strong possibility for an indirect to direct gap transition under a strong electric field in MoSe$_2$.

Results

Indirect to direct band-gap transition under an external electric field. First principles calculations show that electronic band dispersions of bilayer MX$_2$ can be greatly modified by applying an electric field

[1]Department of Physics and Astronomy, Seoul National University, Seoul, 08826, Korea. [2]Center for Correlated Electron Systems, Institute for Basic Science, Seoul, 08826, Korea. [3]Department of Physics, Incheon National University, Incheon, 22012, Korea. [4]Advanced Light Source, Lawrence Berkeley National Laboratory, Berkeley, CA, 94720, USA. [5]Institute of Physics and Applied Physics, Yonsei University, Seoul, 03722, Korea. Correspondence and requests for materials should be addressed to C.K. (email: changyoung@snu.ac.kr) or S.R.P. (email: AbePark@inu.ac.kr)
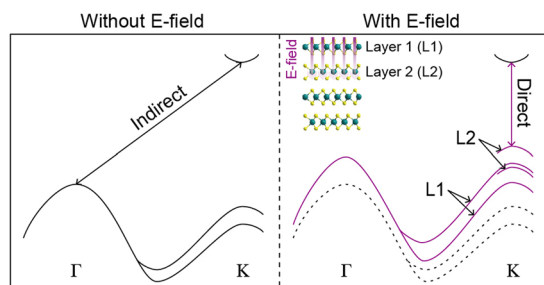
Figure 1. Schematic of electronic structure change in MoSe$_2$ upon application of an electric field. The band structure of MoSe$_2$ along the Γ-K direction without (left) and with (right) an external electric field applied perpendicular to the layers. The nature of the gap is also marked by the arrows. The inset illustrates the crystal structure and an applied electric field. L1 and L2 refer to the surface and sub-surface layers, respectively.

perpendicular to the layers[23]. Bilayer MX$_2$, originally an indirect band gap semiconductor, could even become a metal under a strong electric field. In that process, the location of valence band maximum (VBM) moves from the Γ- (without an electric field) to K-point (with a moderate electric field). This indicates an indirect to direct band gap transition under an electric field even though it was not explicitly discussed in the work due to mis-location of CBM. We point out that recent ARPES experiment results locate CBM at the K-point in MoSe$_2$[4, 32].

Figure 1 illustrates how the band structure of MX$_2$ evolves as an electric field is applied in the calculation results. The band gap is generally reduced but faster at the K-point compared to the Γ-point. Eventually, MX$_2$ will have a direct band gap at the K-point when the field becomes strong enough. Note that only the bands near the K-point are clearly split by the electric field due to the localized character of the wave function within each layer. Electronic states of the lower bands (L2) and upper bands (L1) mainly originate from the surface and sub-surface layers, respectively.

A possible way to induce such a strong electric field on the surface layers of MX$_2$ is by dosing alkali metal on the sample[4, 32, 37, 38]. The electric field is induced by the ionized alkali metal layer when electrons are donated to the sample, and is expected to exist only within the few surface layers of MX$_2$. The electric field strength can be effectively controlled by controlling the alkali metal dosing amount. More importantly, surface sensitive APRES technique can be used to measure the band dispersions.

Electronic structure evolution of MoSe$_2$ by dosing Rb on the surface.

In our experiment, Rb is used for dosing. Figure 2 shows the ARPES data taken along the Γ-K direction for various Rb amounts and dispersions determined from the data. Figure 2(a) shows ARPES data from pristine MoSe$_2$. We can clearly see the valence band structure which is consistent with published results[4]. As the Fermi level (E_F) is in the middle of the gap, we only see the valence band. With a small amount of Rb dosing, electrons are also doped into the sample and E_F shifts to the CBM, causing downward shift of the valence band as seen in Fig. 2(b), compared to the data from the pristine sample in Fig. 2(a). In principle, the very bottom of the conduction band should be visible but the intensity is too weak to be observed.

As the dosing amount increases further, more electrons are doped into the sample and bottom of the conduction band appears at the K-point as well as $\sum$-point (located half way between Γ- and K-points) as seen in Fig. 2(c). The doped electron density (n) can be measured from the Fermi surface volume of the conduction bands and is estimated to be about 2×10^{13} cm^{-2}. Data taken with even more Rb dosing show further downward shift of the conduction band and upward shift for the valence band as plotted in Fig. 2(d) and (e). Here, we note that after formation of Rb monolayer, electron transfer from Rb atom to the system does not occur for the additional Rb dosing on top of Rb monolayer. Therefore, there is a limit in the electron doping concentration using this method. The maximum electron doping we could obtain from the dosing experiment was about $n_{max} \approx 1.4 \times 10^{14}$ cm^{-2} which also sets the maximum induced electric field through the dosing method. The band near E_F at the Γ-point for high n data is the free electron-like Rb band. In order to follow the band dispersion near the K-point, second derivative data is plotted as an inset in Fig. 2(e). Figure 2(f)–(j) plot the band dispersions along the Γ-K direction extracted from the ARPES data in Fig. 2(a)–(e).

There are a few notable aspects of the data. The intensity of the conduction band at the K-point is much stronger compared to that at the $\sum$-point, indicating that the CBM is located at the K-point. As for the valence band, the splitting of the bands to L1 and L2 bands near the K-point (clearly seen in Fig. 2(d)) occurs due to the surface electric field as previously discussed. Overall, the valence band shows an upward shift as seen in Fig. 2(c)–(e) with the doping increase, contrary to what is expected from electron doping. We attribute this behavior to decrease in the band gap size due to the screening effect from the doped carriers[39]. The most important aspect of the dosing dependent band evolution is that the VBM at the K-point rises faster than that at the Γ-point when the surface electron doping increases. As a result, binding energies of the VBM at Γ and K for the maximum electron doping shown in Fig. 2(e) and (j) are almost the same. That is, the system is on the verge of indirect to direct band-gap transition. Readers are reminded that electron doping is directly related to the strength of the electric field.

Focusing on the gap behavior, we plot in Fig. 3(a) the energy positions of VBM at Γ (VB$_\Gamma$), L1 and L2 at K (VB$_{K,L1}$ and VB$_{K,L2}$, respectively) and CBM (CB$_K$) as a function of the electron density. Vertical dotted lines indicate the electron densities for which ARPES data are shown in Fig. 2. VBM position at both Γ and K descends but
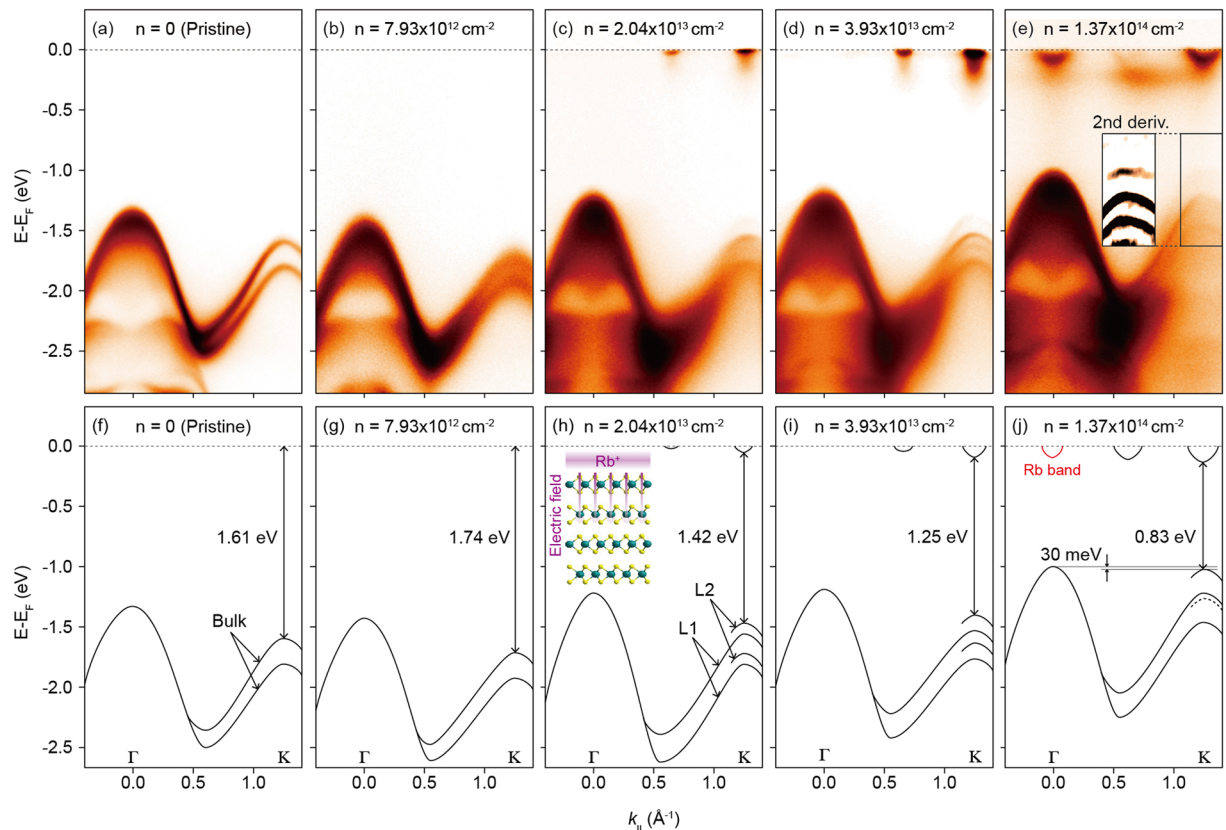
Figure 2. Rb dosing dependent electronic structure of MoSe$_2$. (**a–e**) Γ-K ARPES data as a function of Rb dosing. n indicates the doped electron density as a result of Rb dosing. The inset in panel (**e**) is the second derivative of the boxed K-point data. Shown at the top of the panels are estimated electron densities. (**f–j**) The band structure determined from the ARPES data. The inset in panel (**h**) shows a schematic figure for an electric field in Rb dosed MoSe$_2$. The red solid curve near the Fermi energy in (**j**) denotes the Rb band. The black dashed line in the valence band is the deduced lower L2 band which is not clearly distinguished in the data.

CBM is not seen yet up to electron density of 8×10^{12} cm^{-2}. Therefore, the gap size cannot be determined and the symbols show the energies relative to the Fermi energy. Starting from $n \approx 8 \times 10^{12}$ cm^{-2}, local VBMs at Γ and K begin to ascend while CBM becomes visible and descends as the conduction band is filled. We notice that VB$_{K,L2}$ moves faster than VB$_{\Gamma}$ and almost catches up with VB$_{\Gamma}$ at n_{max}.

More useful information can be obtained by calculating the energy differences among CB$_K$, VB$_{K,L1}$, VB$_{K,L2}$, and VB$_{\Gamma}$ as shown in Fig. 3(b). Note again that we cannot measure the energy in reference to CBM for n lower than 8×10^{12} cm^{-2}. The energy differences Δ^I, Δ^D_{L1} and Δ^D_{L2} (see the caption for the definition) show an initial abrupt decrease right after n $\approx 8 \times 10^{12}$ cm^{-2} but begin to gradually decrease with more doping. Such gap behavior in the doping dependence originates from enhancement of screening effect by doped electrons, which is consistent with recent theoretical calculation results[39].

The energy difference between CB$_K$ and VB$_{\Gamma}$ is smaller than that of CB$_K$ and VB$_{K,L2}$ meaning an indirect band gap semiconductor. However, values for the two are getting closer as n approaches n_{max}. The differences between the direct band gap and indirect band gap sizes as a function of electron doping concentration are plotted in Fig. 3(c). Remarkably, the difference continually decreases with more doping and reveals a fairly linear behavior as shown in Fig. 3(c). This strongly suggest that a stronger electric field which corresponds to 1.5×10^{14} cm^{-2} can induce an indirect to direct band gap transition, as indicated by the vertical dashed line in the figure.

We note a similar work by another group published after we finished our work[40]. They performed ARPES on MoS$_2$, MoSe$_2$, MoTe$_2$, WS$_2$ and WSe$_2$ with Rb dosing and found that only MoTe$_2$ showed the indirect to direct band gap transition. The possible reason that MoSe$_2$ did not show the transition was the insufficient surface doping concentration used in their experiment; we used three times higher surface doping concentration in MoSe$_2$ than in their work and subsequently could reach the point very close to the band gap transition. Overall, our results here are consistent with their work and show that the band gap transition is a general feature of MX$_2$ systems.

Discussion

Rb dosing on the surface has two main effects on the system: surface electron doping and surface electric field. In general, increase in the electron doping enhances screening and reduces the band gap[39]. In fact, it has been already experimentally shown that the gap size of MX$_2$ thin films can be tuned by controlling the screening effect,
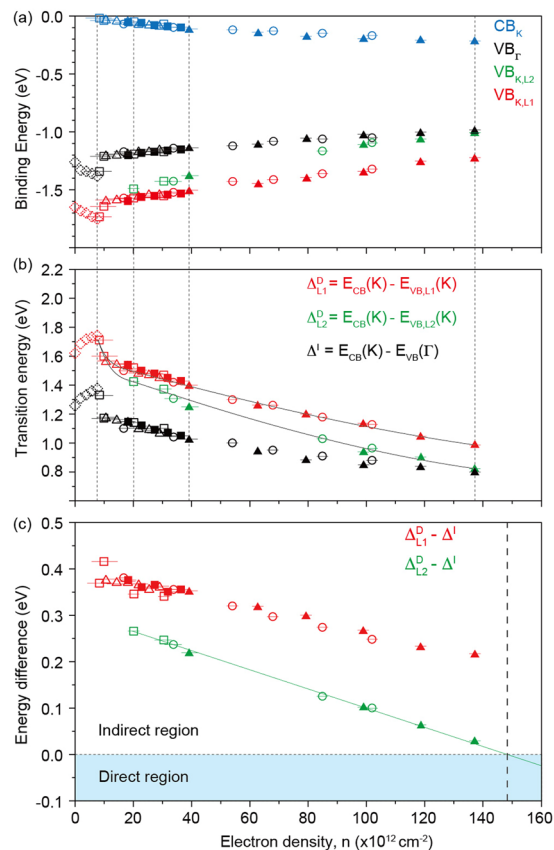
Figure 3. Dosing dependent evolution of the band gap. (**a**) Binding energies of VB_Γ, $VB_{K,L1}$ and $VB_{K,L2}$ as a function of surface doping concentration. CB_K is also shown. Data points drawn with different symbols come from different data sets. Dotted symbols in the low doping region indicate the data from the doping concentration in which CBM could not be observed. Vertical black dotted lines mark the electron densities for the data presented in Fig. 2(b)–(e). (**b**) Doping dependence of the direct gaps $\Delta_{L1}^D = CB_K - VB_{K,L1}$ and $\Delta_{L2}^D = CB_K - VB_{K,L2}$, and indirect gap $\Delta^I = CB_K - VB_\Gamma$. In the low doping region where CBM is not seen, the gap size is referenced to the Fermi energy. (**c**) The differences between the indirect band gap and two direct band gaps at the K-point. A negative value for $\Delta_{L2}^D - \Delta^I$ indicates transition to a direct gap.

for example, by using different substrates[4]. Our experimental results in Fig. 3(b) provides systematic information on this issue. However, it is not intuitively easy to understand that the enhanced screening effect can affect the electronic structure non-uniformly in the momentum space and induce indirect to direct band gap transition. On the other hand, such transition can be attributed to the Stark effect from the surface electric field. The Stark effect can affect electronic states in a momentum dependent way since electronic states can have strong momentum dependence in the orbital character even within the same band. The valence band of MX_2 indeed has momentum dependent orbital character. Not only multilayer but also ML MX_2 show that valence band at K rises faster than the valence band at Γ[23, 26]. The strong Stark effect observed in the semiconducting black phosphorus is similar to what we observed[41]. Therefore, our work proposes a new way to induce direct band gap semiconductor in multilayer MX_2, that is, by applying an electric field. This should be of significant importance for optoelectronics applications of MX_2.

Methods

ARPES measurement. ARPES measurements were performed at the Beam line (BL) 4.0.3 of the Advanced Light Source, Lawrence Berkeley National Laboratory. Surface electron doping was carried out by Rb evaporation on the sample surface using commercial SAES Getters alkali metal dispensers. ARPES spectra were taken with Scienta R8000 electron analyzers. Data were taken with 58 eV photon energy and total energy resolution was better than 20 meV. Samples were cleaved and surface Rb dosing was done at a temperature below 50 K in an ultra-high vacuum better than 5×10^{-11} Torr. All measurements were performed within three hours after cleaving the sample.

Data analysis. The surface electron doping concentration is estimated by calculating the Luttinger area of the conduction band Fermi surfaces at $\sum$ and K, as described in ref. 37. Electrons in the Rb band were not counted. Valley multiplicity of the $\sum$- and K-points are 6 and 2, respectively. In order to calculate the Fermi surface volume, Fermi momentum is determined by fitting the momentum distribution curves at the Fermi energy with a Lorentzian function. For the system in which doping concentration is too low to observe Fermi surfaces clearly,

we assume that the electron doping concentration is proportional to Rb evaporation time. Error bars for electron doping concentrations in Fig. 3 are calculated from the fitting error bars in determining the Fermi momentum. The energy of the CBM at K and the VBM at Γ point is determined from the onset of the photoemission intensity. On the other hand, we use the peak position of the spectrum to determine the energy of the L1 and L2 at the K-point. Error bars for the energy positions in Fig. 3 are smaller than symbols.

References

1. Cheng, R. *et al*. Electroluminescence and photocurrent generation from atomically sharp WSe$_2$/MoS$_2$ heterojunction p-n diodes. *Nano Lett.* **14**, 5590–5597 (2014).
2. Deng, Y. *et al*. Black phosphorus-monolayer MoS$_2$ van der Waals heterojunction p-n diode. *ACS Nano* **8**, 8292–8299 (2014).
3. Xiao, D., Liu, G. B., Feng, W. X., Xu, X. D. & Yao, W. Coupled spin and valley physics in monolayers of MoS$_2$ and other group-VI dicalcogenides. *Phys. Rev. Lett.* **108**, 196802 (2012).
4. Kim, B. S., Rhim, J.-W., Kim, B. Y., Kim, C. & Park, S. R. Determination of the band parameters of bulk 2H-MX$_2$ (M = Mo, W; X = S, Se) by angle-resolved photoemission spectroscopy. *Sci. Rep.* **6**, 36389 (2016).
5. Mak, K. F., McGill, K. L., Park, J. & McEuen, P. L. The valley Hall effect in MoS$_2$ transistors. *Sceince* **344**, 1489–1492 (2014).
6. Lee, J., Mak, K. F. & Shan, J. Electrical control of the valley Hall effect in bilayer MoS$_2$ transistors. *Nat. Nanotech.* **11**, 421–425 (2016).
7. Mak, K. F., Lee, C., Hone, J., Shan, J. & Heinz, T. F. Atomically Thin MoS$_2$: A New Direct-Gap Semiconductor. *Phys. Rev. Lett.* **105**, 136805 (2010).
8. Splendiani, A. *et al*. Emerging photoluminescence in monolayer MoS$_2$. *Nano Lett.* **10**, 1271–1275 (2010).
9. Ye, Z. *et al*. Probing excitonic dark states in single-layer tungsten disulphide. *Nature* **513**, 213–218 (2014).
10. Ugeda, M. M. *et al*. Giant band gap renormalization and excitonic effects in a monolayer transition metal dichalcogenide semiconductor. *Nat. Mater.* **13**, 1091 (2014).
11. Johari, P. & Shenoy, V. B. Tuning the electronic properties of semiconducting transition metal dichalcogenides by applying mechanical strains. *ACS Nano* **6**, 5449–5456 (2012).
12. Lu, N. *et al*. MoS$_2$/MX$_2$ heterobilayers: bandgap engineering via tensile strain or external electric field. *Nanoscale* **6**, 2879 (2014).
13. Conley, H. *et al*. Bandgap engineering of strained monolayer and bilayer MoS$_2$. *Nano Lett.* **13**, 3626–3630 (2013).
14. Horzum, S. *et al*. Phonon softening and direct to indirect band gap crossover in strained single-layer MoSe$_2$. *Phys. Rev. B* **87**, 125415 (2013).
15. Bhattacharyya, S. B. & Singh, A. K. Semiconductor-metal transition in semiconducting bilayer sheets of transition-metal dichalcogenides. *Phys. Rev. B* **86**, 075454 (2012).
16. Shi, H. L., Pan, H., Zhang, Y. W. & Yakobson, B. I. Quasiparticle band structures and optical properties of strained monolayer MoS$_2$ and WS$_2$. *Phys. Rev. B* **87**, 155304 (2013).
17. He, K. L., Poole, C., Mak, K. F. & Shan, J. Experimental demonstration of continuous electronic structure tuning via strain in atomically thin MoS$_2$. *Nano Lett.* **13**, 2931–2936 (2013).
18. Mouri, S. I., Miyauchi, Y. & Matsuda, K. N. Tunable photoluminescence of monolayer MoS$_2$ via chemical doping. *Nano Lett.* **13**, 5944–5948 (2013).
19. Chen, Y. F. *et al*. Tunable band gap photoluminescence from atomically thin transition metal dichalcogenide alloys. *ACS Nano* **7**, 4610–4616 (2013).
20. Mann, J. *et al*. 2-dimensional transition metal dichalcogenides with tunable direct band gaps: MoS$_{2(1−x)}$Se$_{2x}$ monolayers. *Adv. Mater.* **26**, 1399–1404 (2013).
21. Gong, Y. J. *et al*. Band gap engineering and layer-by-layer mapping of selenium-doped molybdenum disulfide. *Nano Lett.* **14**, 442–449 (2014).
22. Su, S.-H. *et al*. Band gap-tunable molybdenum sulfide selenide monolayer alloy. *Small* **10**, 2589–2594 (2014).
23. Ramasubramaniam, A., Naveh, D. & Towe, E. Tunable band gaps in bilayer transition-metal dichalcogenides. *Phys. Rev. B* **84**, 205325 (2011).
24. Yuan, H. T. *et al*. Zeeman-type spin splitting controlled by an electric field. *Nat. Phys.* **9**, 563–569 (2013).
25. Chu, T., Ilatikhameneh, H. D., Klimeck, G. H., Rahman, R. & Chen, Z. H. Electrically tunable bandgaps in bilayer MoS$_2$. *Nano Lett.* **15**, 8000–8007 (2015).
26. Hong, J. S., Lee, C. H., Park, J.-S. & Shim, J. H. Control of valley degeneracy in MoS$_2$ by layer thickness and electric field and its effect on thermoelectric properties. *Phys. Rev. B* **93**, 035445 (2016).
27. Terrones, H., López-Urias, F. & Terrones, M. Novel hetero-layered materials with tunable direct band gaps by sandwiching different metal disulfides and diselenides. *Sci. Rep.* **3**, 1549 (2013).
28. Ma, Z. *et al*. Tunable band structure of heterostructured bilayers with transition-metal dichalcogenide and Mxene monolayer. *J. Phys. Chem. C* **118**, 5593–5599 (2014).
29. Kou, L. Z., Frauenheim, T. & Chen, C. F. Nanoscale multilayer transition-metal dichalcogenide heterostructures: band gap modulation by interfacial strain and spontaneous polarization. *J. Phys. Chem. Lett.* **4**, 1730–1736 (2013).
30. Wei, X.-L. *et al*. Modulating the atomic and electronic structures through alloying and heterostructure of single-layer MoS$_2$. *J. Mater. Chem. A* **2**, 2101–2109 (2014).
31. Song, J.-G. *et al*. Controllable synthesis of molybdenum tungsten disulfide alloy for vertically composition-controlled multilayer. *Nat. Commun.* **6**, 7817 (2015).
32. Zhang, Y. *et al*. Direct observation of the transition from indirect to direct bandgap in atomically thin epitaxial MoSe$_2$. *Nat. Nanotech.* **9**, 111–115 (2014).
33. Jin, W. *et al*. Substrate interactions with suspended and supported monolayer MoS$_2$: angle-resolved photoemission spectroscopy. *Phys. Rev. B* **91**, 121409 (2015).
34. Yeh, P.-C. *et al*. Layer-dependent electronic structure of an atomically heavy two-dimensional dichalcogenide. *Phys. Rev. B* **91**, 041407 (2015).
35. Man, M. K. L. *et al*. Protecting the properties of monolayer MoS$_2$ on silicon based substrates with an atomically thin buffer. *Sci. Rep.* **6**, 20890 (2016).
36. Kim, K. S. *et al*. Coexisting massive and massless Dirac fermions in symmetry-broken bilayer graphene. *Nat. Mater.* **12**, 887–892 (2013).
37. Riley, J. M. *et al*. Negative electronic compressibility and tunable spin splitting in WSe$_2$. *Nat. Nanotech.* **10**, 1043–1047 (2015).
38. Alidoust, N. *et al*. Observation of monolayer valence band spin-orbit effect and induced quantum well states in MoX$_2$. *Nat. Commun.* **5**, 4673 (2014).
39. Liang, Y. F. *et al*. Carrier plasmon induced nonlinear band gap renormalization in two-dimensional semiconductors. *Phys. Rev. Lett.* **114**, 063001 (2015).
40. Kang, M. *et al*. Universal mechanism of band-gap engineering in transition-metal dichalcogenides. *Nano Lett.* **17**, 1610–1615 (2017).
41. Kim, J. M. *et al*. Observation of tunable band gap and anisotropic Dirac semimetal state in black phosphorus. *Science* **349**, 723–726 (2015).

Acknowledgements

Author Contributions

B.S.K., W.S.K., J.J.S. and J.Y.K. performed ARPES measurements with the support from J.D.D.; B.S.K. analyzed the ARPES data; B.S.K., C.K. and S.R.P. wrote the paper; C.K. and S.R.P. are responsible for project direction and planning.

Additional Information

Competing Interests: The authors declare that they have no competing interests.

Publisher's note: Springer Nature remains neutral with regard to jurisdictional claims in published maps and institutional affiliations.